Binding of ATP to UAP56 is necessary for mRNA export

Krishna P. Kota, Stefan R. Wagner, Elvira Huerta, Jean M. Underwood and Jeffrey A. Nickerson*

Department of Cell Biology S7-214, University of Massachusetts Medical School, 55 Lake Avenue, Worcester, MA 01655, USA

*Author for correspondence (e-mail: jeffrey.nickerson@umassmed.edu)

Accepted 11 February 2008
Journal of Cell Science 121, 1526-1537 Published by The Company of Biologists 2008
doi:10.1242/jcs.021055

Summary

The major-histocompatibility-complex protein UAP56 (BAT1) is a DEAD-box helicase that is deposited on mRNA during splicing. UAP56 is retained on spliced mRNA in an exon junction complex (EJC) or, alternatively, with the TREX complex at the 5′ end, where it might facilitate the export of the spliced mRNA to the cytoplasm. Using confocal microscopy, UAP56 was found to be concentrated in RNA-splicing speckled domains of nuclei but was also enriched in adjacent nuclear regions, sites at which most mRNA transcription and splicing occur. At speckled domains, UAP56 was in complexes with the RNA-splicing and -export protein SRm160, and, as measured by FRAP, was in a dynamic binding equilibrium. The application of an in vitro FRAP assay, in which fluorescent nuclear proteins are photobleached in digitonin-extracted cells, revealed that the equilibrium binding of UAP56 in complexes at speckled domains was directly regulated by ATP binding. This was confirmed using a point mutant of UAP56 that did not bind ATP. Point mutation of UAP56 to eliminate ATP binding did not affect RNA splicing, but strongly inhibited the export of mRNA to the cytoplasm.

Supplementary material available online at
http://jcs.biologists.org/cgi/content/full/121/9/1526/DC1

Key words: RNA export, RNA processing, RNA helicase, SRm160, Exon junction complex

Introduction

The gene for the BAT1 protein was first discovered in the human major histocompatibility complex (Spies et al., 1989a; Spies et al., 1989b). BAT1 might be a negative regulator of inflammation, acting by downregulating the production of cytokines, including TNFα, IL1 and IL6 (Allcock et al., 2001). The human BAT1 protein has been identified as an ATP-dependent RNA helicase (Peelman et al., 1995) of the DExD/H family and is homologous to the previously described p47 protein of rat (Nair et al., 1992). Rediscovered as an essential RNA splicing factor, and sometimes renamed UAP56 in mammals (Fleckner et al., 1997), Sub2p in yeast (Libri et al., 2001; Zhang and Green, 2001) and HEL in *Drosophila* (Gatfield et al., 2001), this helicase enables U2 small nuclear ribonucleoprotein (snRNP) attachment to the splicing branch point (Fleckner et al., 1997). In cells, UAP56 is recruited to sites with nascent transcripts in a splicing-dependent manner (Custodio et al., 2004). RNA splicing in both metazoans and yeast requires several helicases of the DExD/H family (reviewed in Staley and Guthrie, 1998; Tanner and Linder, 2001).

RNA splicing is coupled to RNA export from the nucleus; the mRNA produced from intron-containing precursors is exported more efficiently than are identical mRNAs produced without splicing (Luo and Reed, 1999). In one model, this coupling is achieved by the splicing-dependent formation of an exon junction complex (EJC) located at sites 20-24 bases upstream from exon-exon junctions and containing UAP56, the RNA splicing factor SRm160 (SRRM1), RNPS1, Y14, DEK, Aly/REF (Kataoka et al., 2000; Le Hir et al., 2000a; Le Hir et al., 2000b), Magoh (Kataoka et al., 2001), eIF4A3 (Chan et al., 2004), Acinus and SAP18 (Tange et al., 2005). The crystal structure of a core complex with eIF4A3, MLN51, MAGOH and Y14 bound to polyU has been solved (Andersen et al., 2006). In vitro, at least two proteins of the complex, Y14 and Magoh, may bind to the NXF1 (TAP)-p15 heterodimer (Kataoka et al., 2001). Orthologs of NXF1 are essential for the nuclear export of mRNA (Herold et al., 2001; Longman et al., 2003). NXF1 might, in turn, bind directly at nuclear pores (Forler et al., 2004), or bind transportin 2 (karyopherin beta 2b) (Shamsher et al., 2002) for export of the complex from the nucleus.

Some recent data suggests an alternative model in which UAP56 and Aly/REF are associated with a spliced mRNA not at the EJC, but rather as part of the TREX complex, which is recruited to the 5′ end of the mRNA (Cheng et al., 2006). In this model, it is the bound TREX complex that is required for efficient mRNA export and which might interact with NXF1. In addition to UAP56 and Aly/REF, the TREX complex also contains Tex1 and the THO proteins (Jimeno et al., 2002; Reed and Cheng, 2005; Masuda et al., 2005).

At least four RNA helicases with ATPase activity might play roles in mRNA delivery to the cytoplasm. UAP56 orthologs are essential mRNA-export factors in yeast, *Drosophila*, *Xenopus* and *Caenorhabditis elegans* (Gatfield et al., 2001; Jensen et al., 2001; Luo et al., 2001; MacMorris et al., 2003; Strasser and Hurt, 2001), whereas, in human cells, UAP56, or the related protein URH49, are essential for bulk mRNA export (Kapadia et al., 2006). UAP56, and a second putative helicase, Dbp5, bind co-transcriptionally to the Balbiani ring pre-mRNA and remain with the mRNP particle all the way to the nuclear pore (Kiesler et al., 2002; Zhao et al., 2002). Dbp5 might be involved in the release of mRNP at the cytoplasmic face of the nuclear pore (Hodge et al., 1999; Snay-Hodge et al., 1998; Strahm et al., 1999; Tseng et al., 1998). The core of the EJC, which is proposed to be essential for efficient mRNA export, consists of eIF4A3, Y14, Magoh and MLN51 (Ballut et al., 2005). The helicase eIF4E supports the nuclear export of a family of proliferation-related mRNAs sharing a 50-nucleotide

sequence element in their 3′ untranslated region (Culjkovic et al., 2006).

The role of ATP binding, hydrolysis and exchange in the RNA-export functions of these RNA helicases has not been determined. The crystal structure of UAP56 with bound nucleotide has been solved (Shi et al., 2004; Zhao et al., 2004).

We have previously used fluorescence recovery after photobleaching (FRAP) to show an ATP-dependent mobility of the EJC proteins SRm160 and RNPS1 at RNA-splicing speckled domains (Wagner et al., 2004). This was achieved with the use of an in vitro FRAP assay in which fluorescent fusion proteins are photobleached in diginonin-permeabilized cells. Nuclear envelopes remain intact in this assay and molecules small enough to diffuse through nuclear pores, such as ATP, can be added or removed. This assay revealed that SRm160 and RNPS1 are bound at speckled domains, and that ATP, but not its hydrolysis, is required for their release from those binding sites. Because neither protein shows evidence of binding ATP, we hypothesized that they could be released from a complex by an ATP-dependent factor, such as a DEAD-box helicase, that might induce a conformational change without ATP hydrolysis. UAP56 resides in both splicing and RNA-export complexes with SRm160 and RNPS1, making UAP56 a good candidate for mediating their ATP-dependent speckled-domain binding. In addition, the mRNA-binding protein poly(A) binding protein 2 and the mRNA-export factor NXF1 have a FRAP recovery at speckled domains that is slowed by ATP reduction in cells (Calapez et al., 2002). UAP56 is a good candidate for mediating multiple ATP effects on the assembly and functioning of mRNA-export complexes.

In this study, we characterized the cell biology of UAP56, determined its distribution in the nucleus and tracked its redistribution in mitotic cells. Using the technique of FRAP, we characterized the kinetics of UAP56 binding to structures at RNA-splicing speckled domains of the nucleus. In vitro FRAP revealed that the assembly of UAP56 into complexes at RNA-splicing speckled domains required ATP. Using fluorescence resonance energy transfer (FRET), we were able to show that UAP56 and SRm160 inhabit the same complexes at RNA-splicing speckled domains. Mutants of UAP56 with greatly reduced ATP-binding affinity did not affect the ATP-dependent binding of SRm160 at speckled domains. They did, however, inhibit RNA export by a dominant-negative mechanism, showing the central role of ATP binding to UAP56 in mRNA-export-complex assembly.

Results

In order to localize endogenous UAP56 in the nucleus, we generated a rabbit peptide antibody against the GAEPAKKDVKGSYVC internal sequence of UAP56. On a western blot of HeLa and Caski cell lysates, the antiserum detected a single band for each cell line with an approximate molecular mass of 56 kDa, as shown in Fig. 1A. The more-recently discovered URH49 (UAP56 related helicase, 49 kDa) is an RNA helicase that, in humans, has a 90% similarity to UAP56 (Pryor et al., 2004). It contains a sequence that is 62.5% identical (STPAPPKKDIKGSYVS) to our peptide antigen. In order to test whether the polyclonal anti-UAP56 antibody was recognizing this peptide sequence in URH49, either GST-URH49 or GST-UAP56 was expressed in bacteria and affinity purified on Glutathione-Sepharose. Western blotting with the polyclonal antiserum against UAP56 showed that the antibody had a strong preference for UAP56, but at high antibody concentrations there was some crossreactivity with URH49 (Fig. 1B).

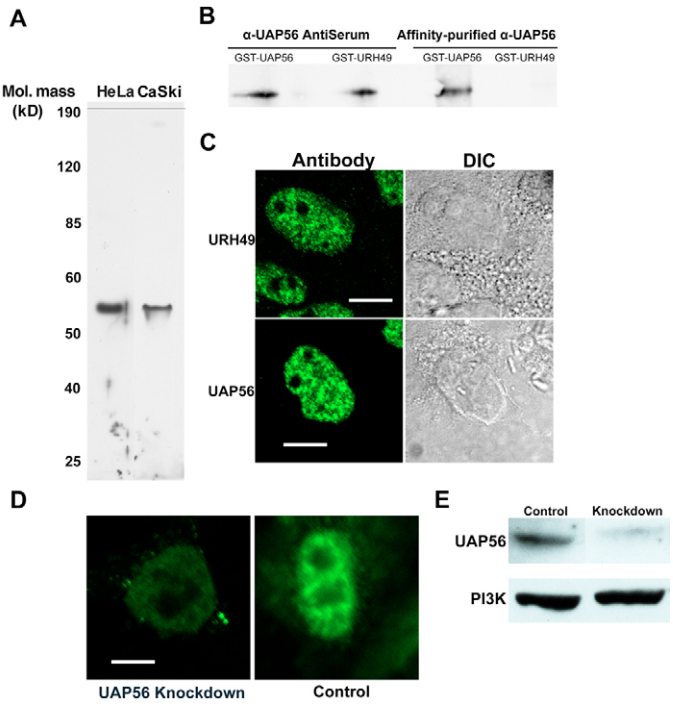

Fig. 1. Affinity purified anti-UAP56 and -URH49 antibodies are highly specific. (A) HeLa and CaSki cell extracts were separated on 10% SDS-PAGE gels probed with unfractionated peptide antibodies generated against UAP56 in rabbit. (B) Affinity purified antibodies detected GST-UAP56 but not GST-URH49. Bacterial lysates containing either GST-UAP56 or GST-URH49 were separated by SDS-PAGE and probed with unfractionated antiserum, which detected both proteins. Affinity purified anti-UAP56 antibody was prepared by passing the antiserum through a GST-URH49 affinity column to remove cross-reacting antibodies. The eluate was then passed through a GST-UAP56 affinity column. Bound antibodies were eluted with glycine HCl, pH 2.0. After affinity purification, the anti-UAP56 antibody detected only GST-UAP56 but not GST-URH49. (C) Affinity purified antibodies against GST-UAP56 and GST-URH49 show that both proteins are located at RNA-splicing speckled domains. HeLa cells were permeabilized, fixed and stained with affinity purified antibodies. (D) HeLa cells were treated with a pool of four siRNA oligonucleotides against UAP56. After 76 hours of treatment, the cells were fixed and immunostained with affinity purified antibodies against UAP56. This treatment removed all detectable UAP56 within the nucleus, demonstrating the high specificity of affinity purified antibody. Both micrographs were collected at the same microscope settings. They are presented as moderately overexposed to show that about 10% of UAP56 remains even after knockdown. Scale bars: 10 μm. (E) The affinity purified anti-UAP56 antibody was used to probe a western blot of protein extracts either from MCF-10A cells treated with a UAP56-specific shRNA knockdown for 76 hours or from control cells. The antibody signal was greatly reduced in the knockdown cells.

To eliminate any possible crossreactions, UAP56-specific antibodies were isolated by affinity purification on immobilized GST-UAP56 after first immunodepleting any crossreacting species on immobilized GST-URH49. Similarly, URH49-specific antibodies were isolated by affinity purification on immobilized GST-URH49 after first immunodepleting crossreacting species on immobilized GST-UAP56. As shown in Fig. 1B, the affinity purified antibodies were specific for their respective antigens. Both affinity purified antibodies were used for the immunofluorescent staining of CaSki cells and they detected both UAP56 and URH49 in the nucleus with a speckled distribution (Fig. 1C). A tenfold higher concentration of anti-URH49 antibody was required for staining. This result, along with the western blot analysis of Fig. 1B, suggested that the crude

antiserum had a greater affinity for UAP56. Immunostaining with antiserum and with affinity purified anti-UAP56 antibodies was indistinguishable by both confocal or electron microscopy in HeLa and CaSki cells, showing that the cellular localization of these similar proteins was the same (data not shown). After using siRNA oligonucleotides to knock down UAP56 levels, but not URH49 levels, immunofluorescent staining with the affinity purified anti-UAP56 antibody was strongly reduced (Fig. 1D). This confirmed the specificity of the antibody for microscopy. After an shRNA-knockdown specific for UAP56 (Kapadia et al., 2006), the western blotting signal generated by the affinity purified antibody was strongly reduced (Fig. 1E).

UAP56 extends outside RNA-splicing speckled domains

Immunofluorescent localization with anti-UAP56 antibodies and confocal microscopy showed that UAP56 was most concentrated in and around RNA-splicing speckled domains (Fig. 2). Inside speckled domains, it colocalized with SRm160, another RNA-splicing and EJC protein (Blencowe et al., 2000; Blencowe et al., 1998; Le Hir et al., 2000b). However, whereas SRm160 was more confined to the speckled domain itself, UAP56 was also enriched in the region around the speckled domain. This is illustrated in Fig. 2B, which presents line scans through six randomly selected speckled domains of the confocal overlay image of Fig. 2A. The profiles of UAP56 (green) across all the speckled domains are broader than those of SRm160 (red). Similar localizations were observed for EGFP-UAP56 and mRFP-SRm160 expressed in cells; both fluorescent fusion proteins colocalized well with their corresponding endogenous proteins (data not shown). Similar results were obtained for cells stained for UAP56 and with SC-35 to mark speckled domains (supplementary material Fig. S1).

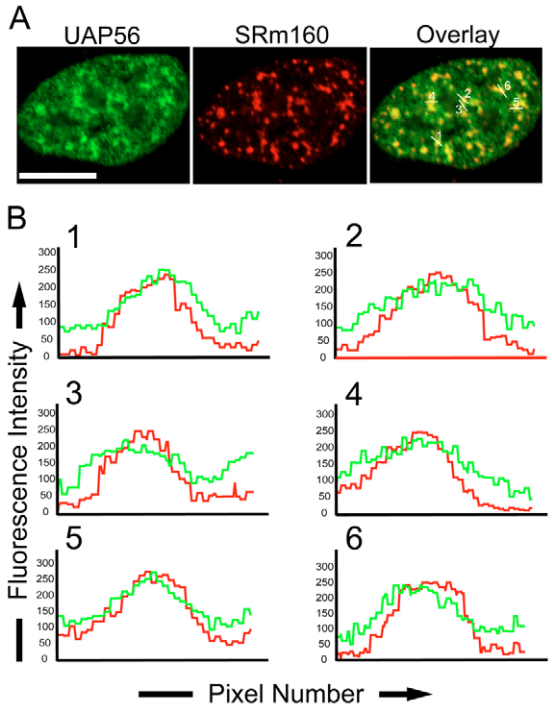

Fig. 2. UAP56 is concentrated in RNA-splicing speckled domains and in the regions surrounding them. (A) CaSki cells were permeabilized, fixed and stained for both UAP56 and SRm160. Confocal microscopy showed that UAP56 was present in RNA-splicing speckled domains, in which it colocalized with SRm160, a well characterized RNA-splicing speckled-domain protein (Blencowe et al., 1998). In the regions around these domains, UAP56 was also present at high concentration, whereas SRm160 was much more confined to the speckled domain itself. Scale bar: 10 μm.
(B) Fluorescence intensity profiles across six randomly selected RNA-splicing speckled domains from the nucleus in A showed that SRm160 was more confined to the speckled domains, whereas UAP56 concentrations extended outside RNA-splicing speckled domains. The *x*-axis represents pixel number along the line passing through the RNA-splicing speckled domain. The fluorescence intensities are plotted along the *y*-axis.

The higher concentration of UAP56 in regions at the periphery of speckled domains was especially evident by electron microscopy (Fig. 3B). At this resolution, each speckled domain consists of an interchromatin granule cluster surrounded by a region enriched in the perichromatin fibrils, which contain many new RNA transcripts (Cmarko et al., 1999; Monneron and Bernhard, 1969). Interestingly, gold beads marking UAP56 were usually present as single beads inside clusters but were often seen in bunches at the periphery. A majority of pre-mRNA transcripts are spliced at or near the periphery of speckled domains (Smith et al., 1999), consistent with the localization of UAP56, and some mRNAs actually move into the interior of these domains before release to the cytoplasm (Shopland et al., 2002).

The mitotic choreography of UAP56

The proteins of RNA-splicing speckled domains segregate to different locations during mitosis before reassembling into structures resembling interchromatin granule clusters at sites outside the reforming nucleus (Ferreira et al., 1994). HEL25E, the *Drosophila* ortholog of UAP56, is essential for normal mitotic spindle assembly in S2 cells, an unexpected result emerging from a genome-wide RNA interference screen (Goshima et al., 2007). Decreasing HEL25E levels results in chromosome misalignment and elongated spindles.

We followed the redistribution of UAP56 through mitosis in HeLa cells, as shown in supplementary material Fig. S2. In all interphase cells, UAP56 was present in 20-40 RNA-splicing speckled domains in the nucleus. In prophase, as chromosomes condensed and the nucleus disassembled, UAP56 retained a speckled distribution, although the speckles were more often at the nuclear periphery or at the edge of condensing chromosomes, as judged by DNA-counterstaining with DRAQ5. By metaphase, UAP56 had moved to the poles of the mitotic spindle and to foci distributed throughout the cytoplasm, but more concentrated around the periphery of the chromosomes. This same distribution is observed for SRm160 at metaphase (Wan et al., 1994), when it might interact with cohesin (McCracken et al., 2005). UAP56 remained at the poles of the mitotic spindle and in smaller cytoplasmic foci through anaphase and into telophase. At telophase, the number of cytoplasmic foci increased and the concentration of UAP56 at the residual spindle pole was less pronounced. By cytokinesis, UAP56 was observed in midbodies as well as in larger structures in the cytoplasm that became entirely nuclear by the end of mitosis. The physical association of UAP56 with the mitotic apparatus and the mitotic defects caused by UAP56-ortholog knockdown in *Drosophila* (Goshima et al., 2007) suggest that UAP56 might play a significant role in spindle regulation.

UAP56 and SRm160 reside in the same complex at RNA-splicing speckled domains

FRET measures the distance between two proteins and can be used to spatially localize sites of interaction in live cells. FRET efficiency decreases with the sixth power of the distance between two

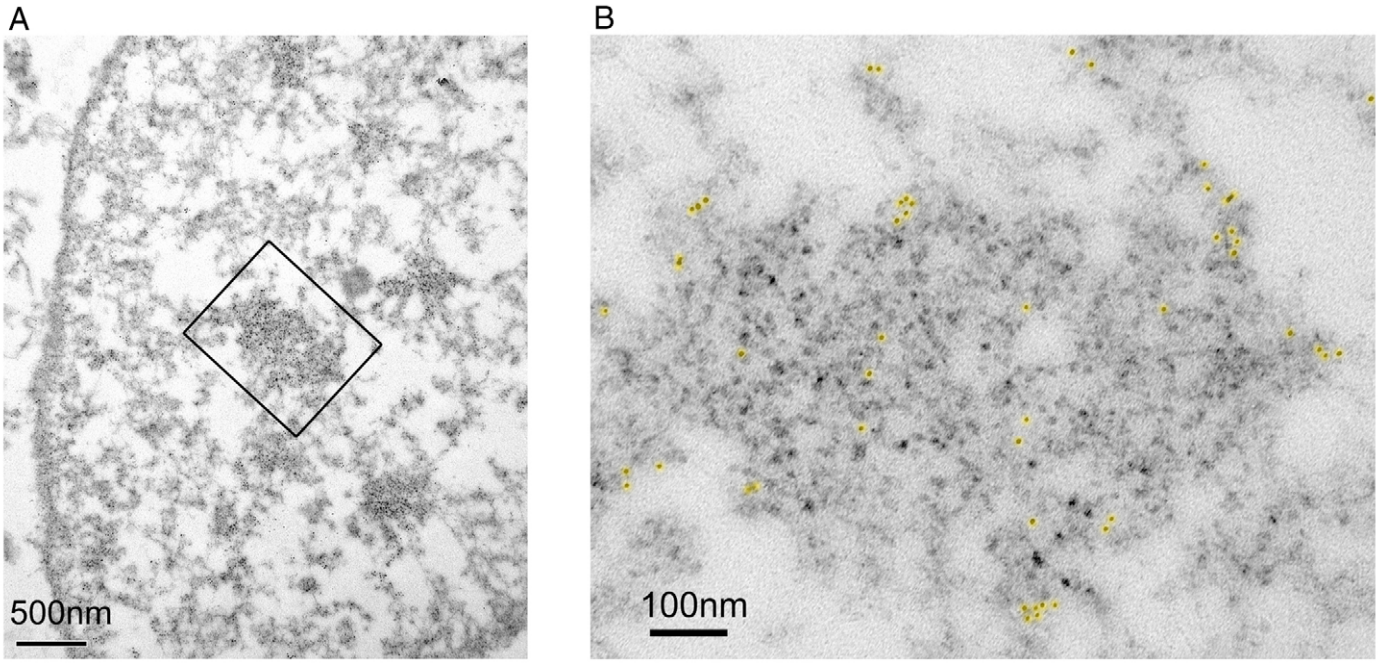

Fig. 3. UAP56 was most concentrated at the periphery of interchromatin granule clusters. Anti-UAP56 antibody and 5 nM gold-bead-conjugated secondary antibodies were used for the pre-embedment staining of CaSki cells with an EDTA regressive counter stain. Although UAP56 was present throughout the cluster, the largest concentration of gold beads was at the periphery of the cluster, where interchromatin granules meet perichromatin fibrils. This is the region of the nucleus in which the majority of transcripts are spliced and from which they are released to the cytoplasm. (A) A low-magnification view of a cell with an EDTA-treatment time of 30 minutes. (B) A high-magnification view of the interchromatin granule cluster indicated in A. The 5-nm gold beads have been highlighted with a yellow overlay to make them easier to distinguish.

fluorophores and, in practice, is only measurable when the distance between them is smaller than 10 nm (Gordon et al., 1998). Although this distance does not assure that the two are direct binding partners, it can establish that the two proteins are present in the same complex. We used mRFP-SRm160 and EGFP-UAP56 as acceptor and donor, respectively.

Analysis with the sensitized emission software of the Leica SP2 confocal system showed that EGFP-UAP56 and mRFP-SRm160 had FRET only in RNA-splicing speckled domains, with FRET efficiencies ranging from 2 to 8% (Fig. 4A). In order to perform these experiments without introducing artifacts, one dish of cells was transfected with only EGFP-UAP56, a second with only mRFP-SRm160 and a third dish with both. At 24 hours after transfection, cells from all three cultures were trypsinized, mixed and replated on coverslips for 24 hours before fixation. Fields in which one cell from each of the transfection conditions was present were selected

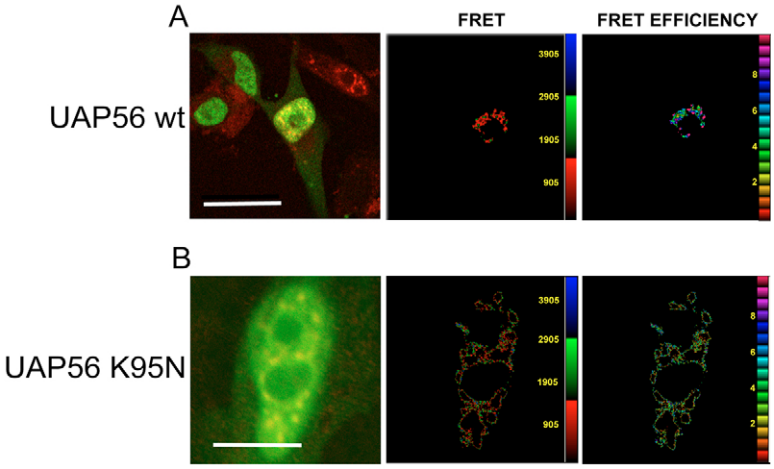

Fig. 4. UAP56 and SRm160 are present in the same macromolecular complexes at RNA-splicing speckled domains. FRET between EGFP-UAP5 wt or UAP56 K95N (green) and mRFP-SRm160 (red) was measured in transiently transfected HeLa cells by the method of sensitized emission (Gordon et al., 1998). (A) Cells expressing both proteins and those expressing only EGFP-UAP56 or only mRFP-SRm160 were trypsinized and replated on coverslips together. Fields that contained at least one co-transfected cell and one each of the control singly transfected cells were selected for analysis (left panel). FRET was found only in cells expressing both EGFP-UAP56 and mRFP-SRm160; within these cells, FRET was found only in the regions of RNA-splicing speckled domains. FRET efficiency was calculated using Leica confocal software. The maximum FRET efficiency between mRFP-SRm160 and EGFP-UAP56 wt at speckled domains was 8%. FRET efficiencies are presented in a color-coded format with a scale to the right of the right panels. (B) There was no FRET observed in RNA-splicing speckled domains between mRFP-SRm160 and EGFP-UAP56 K95N. The maximum FRET efficiency between SRm160 and UAP56 K95N was 6%, but this was in the nucleoplasm. FRET efficiencies are presented in a color-coded format with a scale to the right of the middle panel. Scale bars: 10 μm.

for analysis. The reference images from control cells expressing donor only (EGFP-UAP56) or acceptor only (mRFP-SRm160) and the FRET images from cells expressing both were therefore collected simultaneously under identical optical conditions and from the same field.

When the same experiment was done with EGFP-UAP56 K95N, a mutant that we will show does not bind ATP, and mRFP-SRm160, there was a lower level of FRET in the nucleoplasm but no FRET in RNA-splicing speckled domains (Fig. 4B). In the same experiments, EGFP-Aly/REF and mRFP-SRm160 did not FRET, and EGFP-TAP and mRFP-Y14 did not FRET. Although positive FRET is evidence that two proteins are in the same complex, the absence of FRET is difficult to interpret; two proteins could be sufficiently close but their fluorescent domains might be in the wrong orientation.

These FRET results are consistent with the presence of SRm160 and UAP56 in the same multi-protein complexes located at RNA-splicing speckled domains. Studied in vitro, both proteins can be assembled into RNA-splicing complexes (Blencowe et al., 2000; Blencowe et al., 1998; Blencowe et al., 1994; Fleckner et al., 1997) and are both resident in the EJC (Gatfield et al., 2001; Le Hir et al., 2000a; Le Hir et al., 2000b). Their co-residency in the protein complexes of real cells gives greater biological relevance to those in vitro results.

A point mutation in UAP56 abolishes ATP binding and reduces the spatial association with specked domains

We have previously shown that SRm160 has an ATP-dependent FRAP recovery at RNA-splicing speckled domains (Wagner et al., 2004). Because SRm160 does not have an ATP-binding site, we hypothesized that other proteins would mediate the ATP-dependent incorporation of SRm160 into complexes at speckled domains. SRm160 and UAP56 are present in the same complexes, as shown by extensive in vitro results and by our FRET results (Fig. 4). Because UAP56 has an ATP-binding site, we hypothesized that UAP56 could be the mediator for the ATP-dependent mobilization of SRm160 from RNA-splicing speckled domains. To test this hypothesis, we made a point mutation in the ATP-binding site of UAP56 – a single Lysine to Asparagine substitution at amino acid 95. The crystal structure of UAP56 with bound MgADP (Shi et al., 2004; Zhao et al., 2004) shows that the positively charged Lysine-95 sidechain binds via hydrogen bonds to the oxygen atoms of the β-phosphate of the nucleotide. The same point mutation in the *Saccharomyces cerevisiae* ortholog of UAP56, Sub2p, has previously been used to eliminate ATP binding (Zhang and Green, 2001).

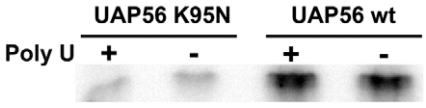

Fig. 5. A point mutation in the ATP-binding domain of UAP56 inhibits ATP binding. A Lysine 95 to Asparagine mutation in the ATP-binding domain of GST-UAP56 was made. Using a method applied to previous DEAD-box helicases (Pause and Sonenberg, 1992), GST-UAP56 wt or GST-UAP56 K95N was UV-cross-linked to bound α-P32-ATP in the presence or absence of 0.1 OD260 units of polyU. The bound and unbound α-P32-ATP were separated on a 12% SDS-PAGE gel before phosphoimaging. The binding of α-P32-ATP was strongly reduced by the mutation but unaffected by polyU.

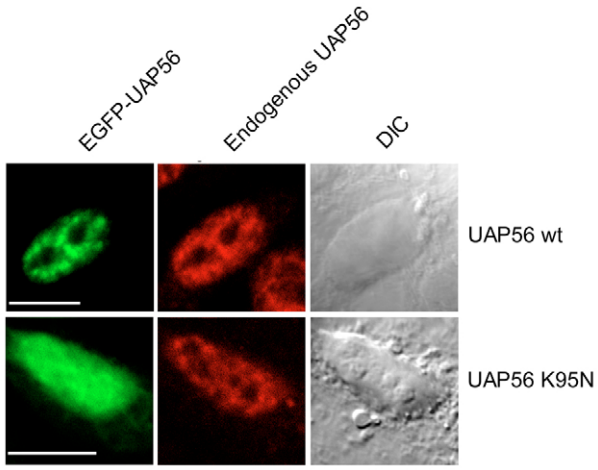

Fig. 6. EGFP-UAP56 K95N was present in higher concentrations in regions outside of the RNA-splicing domains, compared with EGFP-UAP56 wt. HeLa cells were transfected with either EGFP-UAP56 wt or EGFP-UAP56 K95N. At 24 hours after transfection, the cells were fixed, permeabilized and immunostained for endogenous UAP56. Compared with UAP56 wt, UAP56 K95N was less constrained to speckled domains and a higher fraction was present in regions outside the RNA-splicing speckled domains compared with cells expressing UAP56 wt. When stained for endogenous UAP56 protein using affinity purified anti-UAP56 antibody, both proteins localized to RNA-splicing speckled domains along with endogenous UAP56 proteins. Scale bars: 10 μm.

As shown in Fig. 5, the K95N mutation dramatically reduced ATP binding. Adopting a method originally used for the DEAD-box helicase eIF4A (Pause and Sonenberg, 1992), GST-UAP56 or GST-UAP56 K95N were incubated with αP32-ATP and the nucleotide was crosslinked to the active site by ultraviolet irradiation. After SDS-PAGE, the amount of labeled ATP crosslinked to the active site was measured.

The localization of the EGFP-UAP56 K95N mutant was determined by confocal microscopy (Fig. 6). When compared to the wild-type protein, the mutant was more uniformly distributed in the nucleus and not as concentrated at speckled domains. This suggested that UAP56-binding at speckled domains was ATP-dependent. This mutant of UAP56, although not entirely excluded from speckled domains, had no measurable FRET with mRFP-SRm160 at speckled domains (Fig. 4).

Fluorescence recovery after photobleaching

The use of fluorescent fusion proteins makes it possible to characterize the binding and diffusion of proteins within living cells using FRAP and related techniques. For most proteins, fluorescence recovery rates are limited by binding kinetics, which are slower than rates of diffusion (Lele et al., 2004; Lele et al., 2006; Nickerson, 1998). For reference, when considering FRAP results, the half-time ($t_{1/2}$) for the diffusion-limited recovery of EGFP in the nucleus is about 0.2-0.3 seconds (Kruhlak et al., 2000).

When EGFP-UAP56 was expressed in HeLa cells and then the cells were either examined live or fixed before confocal microscopy, it colocalized with the endogenous UAP56 in RNA-splicing speckled domains and also in the region around the speckled domains. This was also the distribution in live cells co-expressing EGFP-UAP56 and mRFP-SRM160. We evaluated the degree of overexpression after transfection by conducting immunofluorescent staining of cells with an affinity purified anti-

UAP56 antibody that recognized both endogenous UAP56 and EGFP-UAP56, and with an Alexa-Fluor-568-conjugated secondary antibody. Total nuclear Alexa-Fluor-568 fluorescence in individual cells was quantified. In relative fluorescence units, EGFP-UAP56-expressing cells had a mean fluorescence of 304±51 (n=10), whereas non-expressing cells had a total fluorescence of 256±11 (n=10). Therefore, the expression of EGFP-UAP56 increased total UAP56 levels by 18.9%.

The binding of UAP56 at RNA-splicing speckled domains was measured in live cells by FRAP of EGFP-UAP56. As shown in Fig. 7A, EGFP-UAP56 recovered at speckled domains with a $t_{1/2}$ of 15.5 seconds. The immobile fraction of 22.5% represented a more tightly bound fraction that did not exchange over the time course of the experiment. We saw no recovery gradient across the bleach zone, consistent with diffusion being much faster than binding or unbinding (Lele et al., 2004). In early experiments, similar recovery curves were obtained for spot and region-of-interest photobleaching, so we routinely used spot photobleaching. We concluded that the recovery rates for both fusion proteins, expressed separately or together, were too slow to be diffusion-limited (Kruhlak et al., 2000; Lele et al., 2004; Lele et al., 2006) and, therefore, the experiment was actually measuring rates of protein exchange at relatively immobile binding sites.

By comparison, EGFP-UAP56 in the nucleoplasm away from speckled domains recovered after spot photobleaching, with a recovery $t_{1/2}$ of 8.8 seconds and an immobile fraction of only 2.5% (n=10, data not shown).

The point mutant EGFP-UAP56 K95N, which had greatly reduced ATP binding, was much less concentrated in and around RNA-splicing speckled domains. It was also less tightly bound to nuclear structures. The mutant had a recovery $t_{1/2}$ of 4.09 seconds with an immobile fraction of 19.1% (Fig. 7A).

We observed a rapid partial decrease in fluorescence intensity outside the bleach zone and this was larger for the mutant protein. This represents a hyperdynamic fraction of protein that is either unbound or very loosely bound (Meshorer et al., 2006). Measured at 2 seconds after the photobleach,

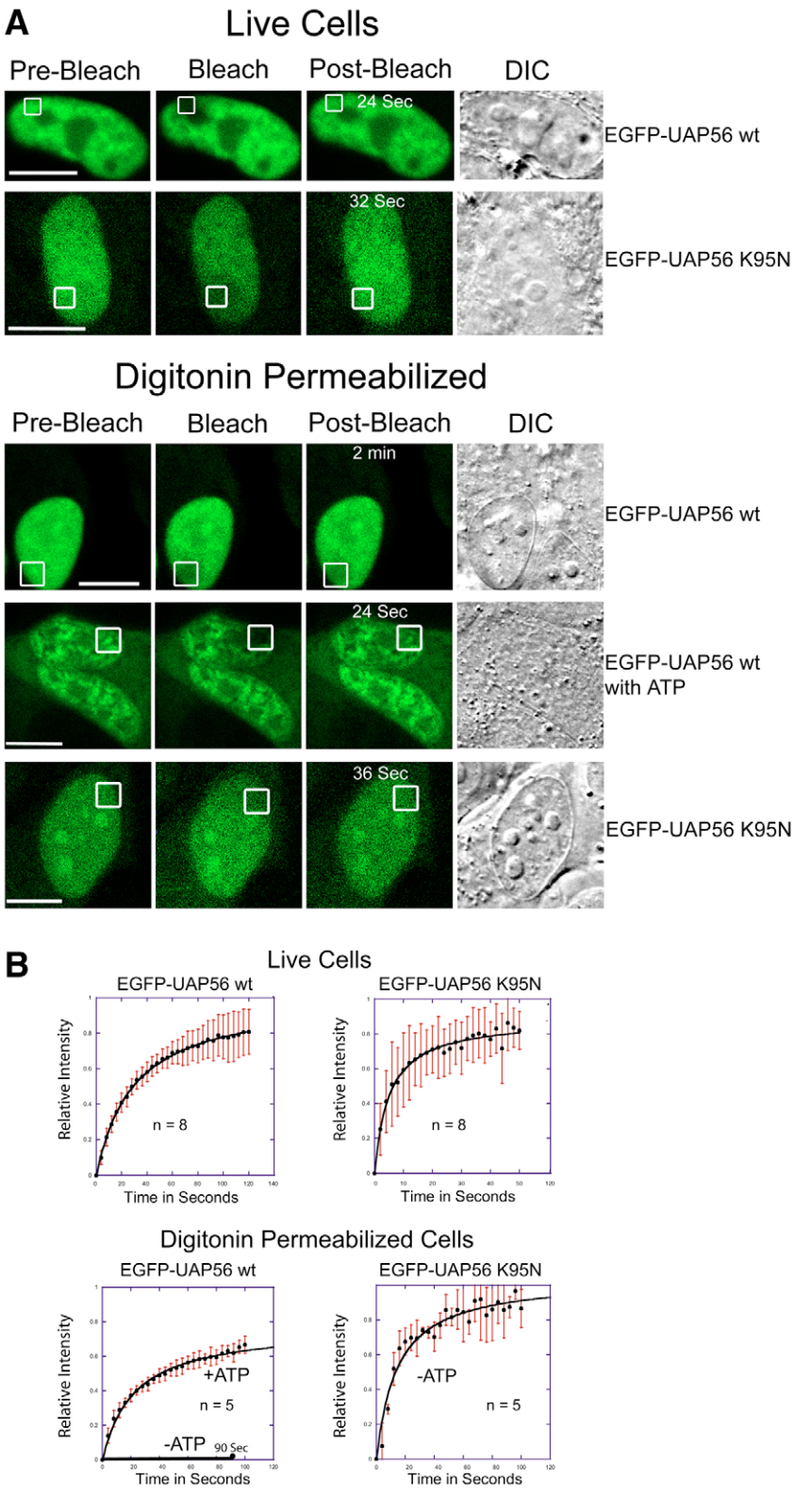

Fig. 7. The FRAP mobility of EGFP-UAP56, but not its K95N mutant, is ATP-dependent. HeLa cells were transfected with EGFP-UAP56 wt or EGFP-UAP56 K95N. After 24 hours, a nuclear region of interest (white square) was photobleached for 3 seconds using maximum laser intensity at 488 nm. The fluorescence recovery of EGFP-UAP56 or its K95N mutant in the bleached zone was recorded. In live cells, the fluorescence of both proteins recovered after photobleaching, showing that UAP56 was exchanging on binding sites at speckled domains. After digitonin permeabilization, the FRAP recovery of EGFP-UAP56 stopped. By contrast, after digitonin permeabilization, EGFP-UAP56 K95N recovered after photobleaching, showing that its exchange at speckled-domain binding sites continued. Addition of 1 mM ATP restored FRAP recovery to EGFP-UAP56, showing that the FRAP mobility, that is the exchange at speckled-domain binding sites, is ATP-dependent. (A) A single cell for each experiment is shown before and after the photobleach, and then at one recovery time point. Scale bars: 10 µm. (B) The calculated recovery curves for all cells in each experiment are shown, with the number of cells (n) noted on each graph. Means are plotted with error bars for standard deviations.

the UAP56 K95N mutant had a hyperdynamic fraction of 32.6±12.9% (n=10), whereas, for wild-type UAP56, it was only 18.4±11.0% (n=10). This change in the size of the rapidly moving pool and the lack of concentration of the K95N mutant at speckled domains suggests that UAP56 binding at speckled domains requires ATP binding.

The UAP56 K95N mutant had a small effect on FRAP recovery rates of mRFP-SRm160 in cells expressing both proteins. mRFP-SRm160 and EGFP-UAP56 K95N, the ATP-binding deficient mutant of UAP56, were co-expressed in HeLa cells. After 16 hours, the binding of SRm160 at RNA-splicing speckled domains was measured in live cells by FRAP (Fig. 8). In cells expressing mRFP-SRm160, recovery had a $t_{1/2}$ of 16.3 seconds, similar to the rate of EGFP-SRm160 recovery (Wagner et al., 2004). The immobile fraction was 11%, and this represents a fraction of SRm160 that was so tightly bound that it did not exchange over the time course of the experiment.

Co-expression with either wild-type EGFP-UAP56 (EGFP-UAP56 wt) or the EGFP-UAP56 K95N mutant increased the size of the immobile fraction of mRFP-SRm160 (Fig. 8). This was 22% of the mRFP-SRm160 for cells co-expressing EGFP-UAP56 wt and 27.5% for cells also expressing EGFP-UAP56 K95N. In the presence of either EGFP-UAP56 wt or mutant EGFP-UAP56 K95N, mRFP-SRm160 recovered with a $t_{1/2}$ of 6.1 seconds. This was more than twice as fast as in control cells expressing neither form of UAP56 (Fig. 8B). There was no significant difference between the recovery curve for mRFP-SRm160 in the presence of EGFP-UAP56 wt compared to the recovery of mRFP-SRm160 in the presence of EGFP-UAP56 K95N (P<0.995).

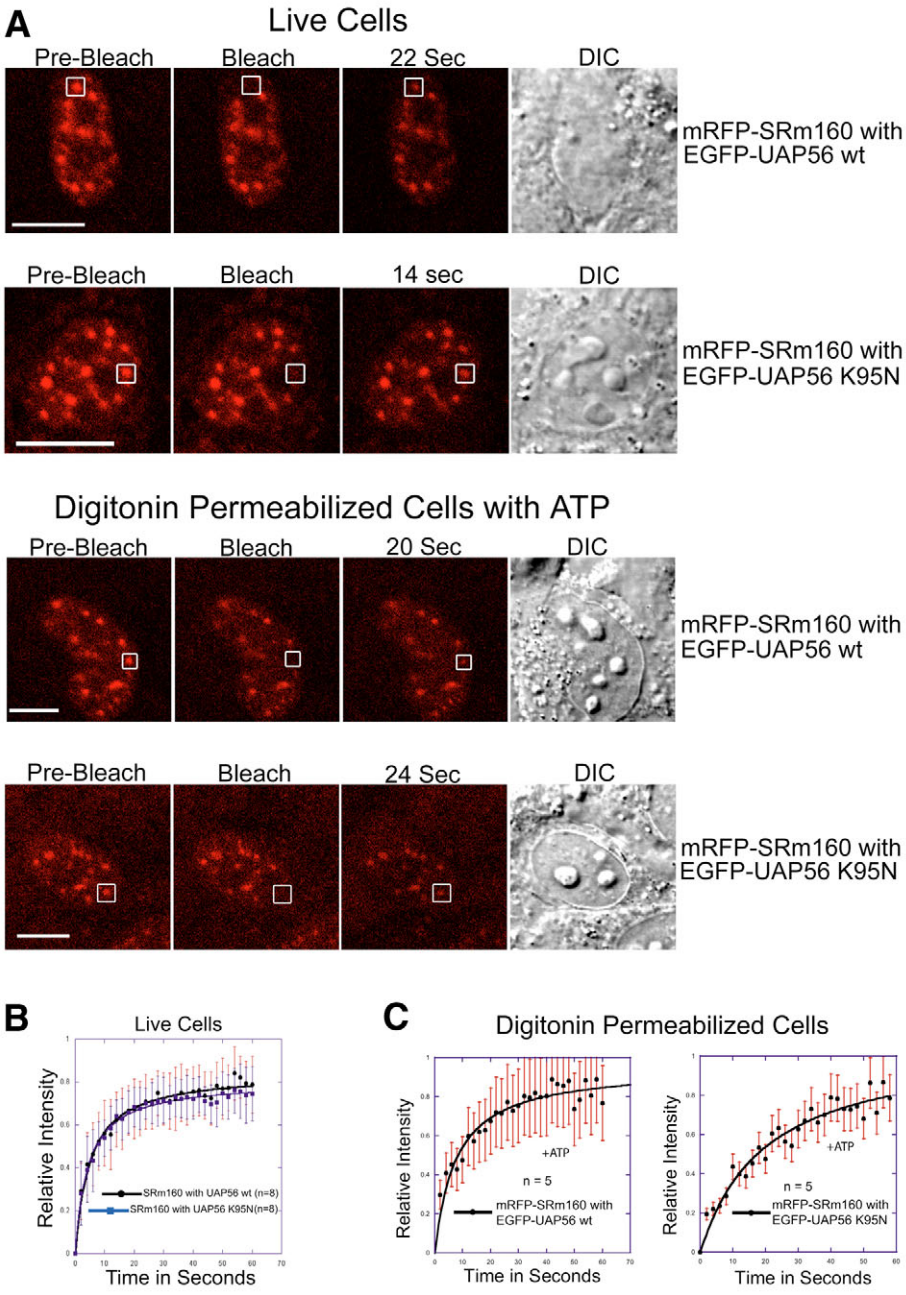

UAP56 K95N does not affect the ATP-dependence of SRm160 binding

We have developed a novel assay for measuring the effects of small molecules on the binding of fluorescent fusion proteins in nuclei (Wagner et al., 2004). In this 'in vitro FRAP' technique, cells are permeabilized with digitonin, which leaves the nuclear envelope intact. Small molecules diffuse through nuclear pores, while the nuclear envelope retains larger molecules and their complexes. Thus, small molecules can be easily removed or added back. Using this technique, we showed that ATP quickly leaves the nucleus after digitonin permeabilization (Wagner et al., 2004). As a result, EGFP-SRm160 does not recover when photobleached at speckled domains in the nuclei of digitonin-treated cells. Adding back ATP restores recovery,

Fig. 8. UAP56 does not mediate the ATP-dependent intra-nuclear mobility of SRm160. HeLa cells were co-transfected with mRFP-SRm160 and either EGFP-UAP56 wt or EGFP-UAP56 K95N. After 24 hours, the mRFP-SRm160 in a nuclear region of interest (white square) was photobleached for 3 seconds using maximum laser intensity at 568 nm. The recovery of mRFP-SRm160 in the bleached zone was recorded. The cells were later permeabilized with digitonin, which permeabilizes the cell membrane but leaves the nuclear envelope intact. When digitonin-permeabilized cells were photobleached, there was no recovery of fluorescence in the bleached zone (data not shown) (Wagner et al., 2004). Adding back 1 mM ATP restored fluorescence in cells expressing either wild-type UAP56 or UAP56 K95N. The ATP-dependence of SRm160 exchange at speckled domains did not depend on the ability of UAP56 to bind ATP. (A) A single cell for each experiment is shown before and after the photobleach, and then at one recovery time point. Scale bars: 10 μm. (B) The calculated recovery curves for all cells in each live-cell experiment are shown with the number of cells noted on each graph. (C) Matching calculated results for in vitro FRAP experiments in which the cells were digitonin-permeabilized before photobleaching. The error bars are standard deviations.

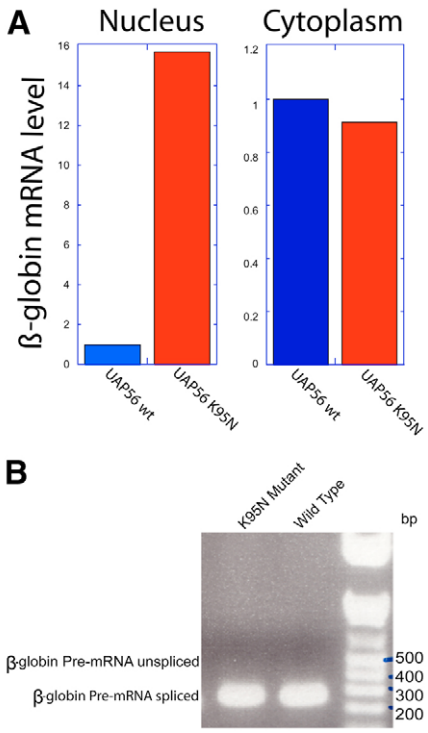

Fig. 9. UAP56 K95N has a dominant-negative effect on RNA export. 293T cells were co-transfected with a β-globin-splicing reporter plasmid and EGFP-UAP56 wt or EGFP-UAP56 K95N expression vector. 24 hours after transfection, the RNA of the cells was separated into cytoplasmic and nuclear fractions. Real-time PCR with primers recognizing the 5′ exon and 3′ exon was performed. (A) In cells expressing EGFP-UAP56 K95N, there was a 15-fold increase of β-globin in the nuclear fraction compared with cells expressing EGFP-UAP56 wt. (B) When the nuclear PCR product was separated on a 1% agarose gel it was all spliced, showing that the nuclear accumulation is due to reduced mRNA export and not pre-mRNA splicing.

showing that the exchange of SRm160 at speckled domains requires ATP. Because SRm160 does not have an ATP binding site and since it is in complexes with UAP56 which does have an ATP-binding site, we hypothesized that UAP56 might mediate the ATP-dependent binding of SRm160 at speckled domains.

After digitonin permeabilization to remove ATP, mRFP-SRm160 did not recover after photobleaching at speckled domains. This was consistent with the results we have previously reported for EGFP-SRm160 (Wagner et al., 2004). Photobleach recovery could be restored by adding back 1 mM ATP (Fig. 8). There was no effect on the ATP-dependence of SRm160 recovery when EGFP-UAP56 or EGFP-UAP56 K95N were also present. The ATP-dependent recovery of mRFP-SRm160 was slightly faster in the cells expressing EGFP-UAP56 K95N ($t_{1/2}$=13.1 seconds) than in the cells expressing the wild-type EGFP-UAP56 ($t_{1/2}$=15.5 seconds). The immobile fractions were similar after ATP supplementation and were about 20%.

In earlier experiments, we observed no effect on the ATP-dependent FRAP recovery of EGFP-SRm160 in live cells after partial RNAi knockdown (Fig. 1D) of UAP56 (data not shown). Knockdown of UAP56 alone is, however, insufficient to strongly inhibit mRNA export, apparently because it can be replaced by URH49 (Kapadia et al., 2006).

The binding of wild type UAP56 at speckled domains requires ATP

The UAP56 in live cells was in rapid equilibrium between a diffusing pool and a fraction bound at RNA-splicing speckled domains; the $t_{1/2}$ of exchange on speckled domains was 15.5 seconds (Fig. 7). However, after permeabilization of the nuclear envelope, UAP56 remained tightly bound at speckled domains and was not removed even after 5 minutes (Fig. 2). This discrepancy suggested that UAP56 binding and exchange at speckled domains might require a cofactor that was removed by permeabilization. Because UAP56 K95N, which did not bind ATP, did not localize well to speckled domains (Fig. 6), the likely cofactor was ATP. The in vitro FRAP assay was used to test the hypothesis that ATP was required for the exchange UAP56 at speckled domains (Fig. 7). In digitonin-permeabilized cells, which are depleted of ATP (Wagner et al., 2004), EGFP-UAP56 did not recover after photobleaching. When 1 mM ATP was added back, recovery was restored with a $t_{1/2}$ of 16.4 seconds and an immobile fraction of 34.4%. Because the UAP56 K95N mutant, which cannot bind ATP, does not concentrate in speckled domains, we conclude that ATP is affecting the on-rate constant for UAP56 binding in complexes at speckled domains.

RNA export to the cytoplasm requires binding of ATP to UAP56

UAP56 and its orthologs are essential mRNA export factors in yeast, *Drosophila*, *Xenopus* and human cells (Gatfield et al., 2001; Jensen et al., 2001; Kapadia et al., 2006; Luo et al., 2001; Strasser and Hurt, 2001). To test the hypothesis that UAP56 ATP-binding activity is required for the export of mRNA, we transiently transfected 293T cells with an intron-containing β-globin minigene and either wild-type EGFP-UAP56 or the EGFP-UAP56 K95N mutant. After 24 hours, cytoplasmic and nuclear RNA was separated and extracted. Using quantitative reverse transcriptase (RT)-PCR, the relative concentrations of spliced and unspliced β-globin RNA were measured in each fraction. As shown in Fig. 9A, cells expressing the ATP-binding mutant, UAP56 K95N, accumulated spliced β-globin mRNA in their nuclei to a level 15-fold higher than in nuclei of cells expressing wild-type UAP56. The level of unspliced β-globin RNA in the nucleus was not significantly changed by the K95N mutant (Fig. 9B).

In previous work, the knockdown of UAP56 caused some nuclear accumulation of poly(A) RNA (Kapadia et al., 2006). The inhibition of mRNA export was stronger when both UAP56 and the related protein URH49 were knocked down, showing that the two proteins can perform redundant functions in RNA export. The double knockdown was quickly lethal. The results that we report here are consistent with ATP playing an essential role in the RNA-export function of UAP56. The effect of expressing UAP56 K95N was much greater than that of knocking down UAP56, suggesting that the UAP56 K95N mutant has a dominant-negative effect, affecting both the UAP56 and the URH49 RNA-export mechanisms.

Discussion

UAP56 is concentrated in splicing speckled domains but is also enriched in the surrounding perispeckle region (Figs 2, 3). This is consistent with a role for UAP56 in RNA splicing and export, because a majority of transcripts are spliced in sites at or near splicing speckled domains (Smith et al., 1999). Imaged by electron microscopy, each domain consists of a cluster of granules called an interchromatin granule cluster surrounded by a region enriched in perichromatin fibrils (Monneron and Bernhard, 1969). The

clusters contain high concentrations of RNA-splicing factors (Lamond and Spector, 2003; Mintz et al., 1999; Saitoh et al., 2004), whereas perichromatin fibrils contain many new RNA transcripts (Biggiogera and Fakan, 1998; Cmarko et al., 1999). Some mRNAs might traffic through both regions, moving from the periphery into the interior of a speckled domain before release to the cytoplasm (Shopland et al., 2002).

In vitro assays have previously shown that UAP56 and SRm160 are both present in spliceosomes and are both present in the EJC, which is proposed to facilitate efficient RNA export out of the nucleus. Here, we used FRET to establish the presence of both proteins in the same complexes located at RNA-splicing speckled domains of the nucleus (Fig. 4). The formation of complexes of proteins implicated in RNA export has not previously been established by FRET. FRET between two fluorophores occurs only when the distance between them is in the range of 1-10 nM (Gordon et al., 1998). At this distance, we can be assured that both proteins are present within the same complex. Bimolecular fluorescence complementation has been used to show that two other EJC proteins – Y14 and NXF1 (TAP) – inhabit the same complex in cells (Schmidt et al., 2006). Bimolecular complementation provides a stronger signal but, because it requires a more stable complex in which fluorescence develops over a period of one to several hours, more dynamic events might be missed.

FRET between EGFP-UAP56 and mRFP-SRm160 occurred only within RNA-splicing speckled domains and with a maximum FRET efficiency of 8%. This is a high efficiency for this technique and suggests that the two proteins are close together within the same complex. FRET can be difficult to establish because it depends on the distance between, orientation of and environment of the two molecules. However, the importance of attempting to establish which complexes exist in cells, and at which sites, is emphasized by a recent proteomic study identifying proteins co-immunoprecipitating with anti-SRm160 antibodies (McCracken et al., 2005). There were 110 co-immunoprecipitating proteins identified. Theoretically, by including a single SRm160 molecule in each complex, we could assemble 110 different dimers, 12,100 different trimers, more than 1.3 million tetramers, and so on. It is important to supplement the powerful techniques of in vitro biochemistry with experimental approaches that detect complexes, such as the one including UAP56 and SRm160, that actually form in cells.

The physical chemistry of binding – including the measurement of kinetic parameters, of equilibrium constants and of the sizes of bound versus diffusing pools – is readily studied in live cells by the complimentary technique of FRAP or its variants (Kruhlak et al., 2000; Lele et al., 2004; Lele et al., 2006; Lele and Ingber, 2006; Phair and Misteli, 2000; Phair et al., 2004; Stenoien et al., 2001). FRAP has shown that the binding of other RNA-splicing factors and RNA-export factors in splicing speckled domains is dynamic (Kruhlak et al., 2000; Phair and Misteli, 2000; Wagner et al., 2004). Factors cycle into and out of speckles, although the shape and position of the speckles remains constant over time periods of many minutes. We report similar behavior for UAP56.

UAP56 binds and hydrolyses ATP (Shi et al., 2004). We engineered a point mutation in the ATP-binding site of UAP56 that inhibited ATP binding (Fig. 5). This UAP56 K95N mutant did not affect mRNA splicing, but had a dominant-negative effect on nuclear export of mRNA (Fig. 9). The mechanism for this effect on mRNA export might be that the binding of ATP to UAP56 is required for UAP56 incorporation into mRNA-export complexes at RNA-splicing speckled domains. First, the K95N mutation in the ATP-binding site made the protein less concentrated in RNA-splicing speckled domains (Fig. 6). Second, during in vitro FRAP experiments, wild-type UAP56 did not recover after photobleaching in the absence of ATP (Fig. 7). Photobleach recovery was restored by adding back ATP, and with kinetics similar to those seen in live cells. Expression of this mutant UAP56 did not change the ATP-dependence of SRm160 binding at RNA-splicing speckled domains (Fig. 8), even though UAP56 and SRm160 were present in the same complexes (Fig. 4).

The simplest model we can propose based on the FRET and FRAP results we report here, supplemented by previous in vitro results, is that UAP56, SRm160 and RNPS1 are present in the same complex at speckled domains and that the assembly of this complex has two ATP-dependent steps: one for the incorporation of UAP56 in the complex and a second for the incorporation of SRm160. The first step is mediated by the binding of ATP to UAP56, whereas the second is mediated by the binding of ATP to a factor that is yet to be identified. Assembly of the complex is required for mRNA export.

Recent advances in microscopy have given us a new set of tools for studying biochemistry in real cells. We recommend in vitro FRAP as an additional tool for identifying cofactors, such as ATP, that are required for complex assembly and disassembly. With the complimentary use of protein knockdowns, protein mutations and cofactor analogs, the in vitro FRAP technique allows us to probe deeper into the mechanisms of complex assembly in the context of a real cell.

Materials and Methods

Constructs

GST-UAP56 and GST-URH49 vectors (Kapadia et al., 2006) were a gift from Lee Johnson (Ohio State University, Columbus, OH). For generating green fluorescent UAP56, the cDNA was amplified by high fidelity PCR, sequenced, and then cloned into EGFP C1 vector (Clontech). Similarly, the mRFP-SRm160 was generated by amplifying the cDNA as above and transferred into an expression vector containing mRFP. Briefly, the vector was based on EGFP-C2 (Clontech) but with the EGFP replaced with mRFP from a cDNA provided by Roger Tsien (University of California, San Diego, CA).

UAP56 K95N with a point mutation in the UAP56 ATP-binding site was made using a Stratagene QuikChange site-directed mutagenesis kit. Mutations at desired sites were confirmed by DNA sequencing.

Transfections

HeLa cells (at ~75% confluence) on 22×22-mm coverslips were transfected with 6 μg of plasmid DNA encoding EGFP-UAP56 wt or EGFP-UAP56 K95N and/or mRFP-SRm160 using 15 μl of Lipofectamine 2000 per coverslip in 1 ml of Optimem (GiboBRL, Life Science Research, Paisley, UK) for 4 hours and then the medium was replaced with DMEM complete medium with 10% FBS. After overnight culture, the transfection efficiency was >75%.

Generation of UAP56 antibodies

A hexadecapeptide contained within human UAP56 (GAEAPAKKDVKGSYVC) was synthesized and coupled to Keyhole Limpet Hemocynanin (SynPep, Dublin, CA). Rabbit antiserum was prepared by Covance (Denver, PA).

Affinity purification of antibodies

The GST-UAP56 and GST-URH49 fusion proteins were purified and bound to Glutathione-Sepharose 4B beads (Novagen) as described previously (Pryor et al., 2004), except that the volume of beads used was 100 μl. The protein-bound resins were washed three times with cross-linking buffer (200 mM HEPES, pH 8.5) and then cross-linked with 2 ml of 20 mM Dimethy Pimelimidate (Sigma) in cross-linking buffer for 1 hour at room temperature. The cross-linking solution was removed by centrifugation at 500 ***g*** for 2 minutes and residual cross-linker was neutralized by adding 2 ml of 200 mM Ethanolamine (Sigma) for 30 minutes at room temperature. Non-covalently bound molecules from the resin were removed by washing twice with 2 ml of glycine elution buffer (150 mM NaCl, 200 mM Glycine-HCl, pH 2.0). Finally, the resin was washed with 10 ml of TBS twice at 4°C. The antibodies were diluted with 1:1 TBS and mixed with GST cross-linked resin for 30 minutes at 4°C.

The unbound antibodies were removed by centrifugation at 500 ***g*** for 2 minutes. The resin was washed with 5 volumes of TBS, and with 10 volumes of wash buffer (500 mM NaCl, 20 mM Tris, pH 7.4, 0.1% Triton X-100). The antibodies were eluted with 2 ml of glycine elution buffer.

Immunocytochemistry

To prepare cells for immunofluorescent localization experiments, two different methods were applied:

(1) Fixation/permeabilization: cells were washed in PBS before fixation with 4% formaldehyde in cytoskeletal buffer (10 mM Pipes, pH 6.8/300 mM sucrose/100 mM NaCl/3 mM $MgCl_2$/1 mM EGTA) for 50 minutes. To improve antibody penetration, the cells were then permeabilized using 0.5% Triton X-100 in cytoskeletal buffer for 5 minutes. All steps were performed at 4°C.

(2) Permeabilization/fixation: after washing in PBS, cells were incubated in 0.5% Triton X-100 in cytoskeletal buffer for 2-5 minutes. This step removes soluble proteins from both the cytoplasm and nucleus. Cells were later fixed in 4% formaldehyde in cytoskeletal buffer for 50 minutes. All steps were performed at 4°C.

Antibody staining: cells were stained with antibodies as described (Wagner et al., 2003) and, unless otherwise specified, imaged with a Leica SP1 laser scanning confocal microscope. The B1C8 monoclonal antibody against SRm160 is available from Calbiochem/EMD. The SC-35 monoclonal was from Sigma. Line profiles through speckled domains were measured using ImageJ.

Western blots

Proteins from HeLa and CaSki cell lysates were separated by 10% SDS Gel electrophoresis, and transferred to nitrocellulose membranes. Western blots were performed using primary antibodies raised against UAP56 in rabbit or affinity purified URH49 or UAP56 antibodies, followed by Goat anti-rabbit horseradish peroxidase conjugated secondary antibodies, and developed with SuperSignal West Pico Chemiluminescent Substrate (Pierce, Rockford, IL).

Pre-embedment electron microscopic localization of UAP56

CaSki cells were grown on Thermanox coverslips (Nunc). The cells were washed at 4°C in PBS, permeabilized with cytoskeletal buffer containing 0.5% Triton X-100, 2 mM VRC (vanadyl ribonucleoside complex) and 1 mM AEBSF [4-(2-aminoethyl)-benzenesulfonyl fluoride, hydrochloride] at 4°C for 5 minutes, fixed in 4% paraformaldehyde (Ted Pella) in cytoskeletal buffer containing VRC and AEBSF at 4°C for 40 minutes, washed twice in cytoskeletal buffer at 4°C, then antibody-stained with a rabbit antibody against UAP56. Control sections were not exposed to the first antibody. The second antibody was linked to 5-nm gold beads (Nickerson et al., 1990). Cells were then fixed with 2.5% glutaraldehyde (Ted Pella) in 0.1 M Sörensen's phosphate buffer, pH 7.3 (Glauert, 1991) at 4°C for 1 hour, then washed twice in the same buffer and held overnight at 4°C in the buffer. Cells were dehydrated in a graded series of ethanol solutions with propylene oxide as the intermediate solvent, infiltrated with and embedded in Epon/Araldite, and cured at 60°C for 2 days. The coverslips were removed and thin sections were cut. The sections were EDTA regressively stained (Bernhard, 1969) with 5% uranyl acetate for 3 minutes, 0.2 M EDTA for 30-60 minutes and then lead-citrate stained (Knight, 1982) for 2.5 minutes. Sections were imaged with a Philips CM10 electron microscope with a Gatan ES1000W Erlangshen CCD Camera.

Fluorescence recovery after photobleaching

FRAP was performed at 37°C as described previously (Wagner et al., 2004). Routinely, two images were taken before and 20-30 images were taken after the bleach at intervals of 1-20 seconds depending on the time of recovery. To destroy EGFP fluorescence, maximal laser power was applied to a region of interest for 3 seconds. Confocal Software (version 2; Leica Microsystems) was used to measure the intensity of fluorescence in the bleached area and in the whole nucleus for the whole stack of images. For analysis, these data were transferred into a Microsoft Excel spreadsheet. Any remaining fluorescence in the bleached area after the bleach was normalized to zero. The relative fluorescence intensity (I_{rel}) in the bleached area was calculated as described previously (Phair and Misteli, 2000). $I_{rel}=T_0\, I_f/T_t\, I_0$, with T_0 being the total cellular fluorescence before bleach, T_t the total cellular fluorescence at time t, I_0 the fluorescence in the bleached area before bleach, and I_f the fluorescence in the bleached area at time t. Recovery curves were drawn using Kaleidagraph 3.5 (Synergy Development). The percentage of immobile protein was determined after normalization of fluorescence in the bleached area to 0 in the first post-bleach image and 1 in the pre-bleached image, and it was calculated as the percentage difference between the relative fluorescence asymptote of the recovery curve and a relative recovery of 1, a value that would reflect complete recovery without an immobile fraction. For example, an asymptote at 0.8 reflects an immobile fraction of 20%. Curve-fitting for graphic presentation was performed as described previously (Liu et al., 2005). Individual time points are presented as means with error bars showing standard deviations. Half times of recovery were obtained from individual fitted recovery curves when the relative recovery reached half of the plateau value minus the initial value after the bleach.

In vitro FRAP assays

We have previously reported the development of an assay for measuring the effect that molecules small enough to diffuse through nuclear pores have on the binding of nuclear proteins to nuclear structures such as chromatin or RNA-splicing speckled domains (Wagner et al., 2004). Fluorescent-protein-expressing cells were grown on 40-mm diameter circular coverslips. After viewing coverslips in a Bioptechs FCS2 live-cell chamber on the Leica SP1 confocal microscope with a Bioptechs objective heater, cells were perfused with permeabilization buffer (20 mM HEPES, pH 7.3; 110 mM potassium acetate; 2 mM magnesium acetate). Cells were then permeabilized by perfusion with 50 μg/ml digitonin in permeabilization buffer for 6 minutes. After incubation, the cells were washed again with permeabilization buffer. FRAP kinetic measurements were made as described above. To examine the effect of ATP on the recovery of fluorescent-tagged proteins, a stock solution of 1 mM ATP was freshly made in permeabilization buffer with the pH readjusted to 6.8. Different ATP concentrations in permeabilization buffer were perfused onto digitonin-permeabilized cells, in which ATP equilibrated across nuclear pores, and then FRAP recovery rates for nuclear proteins were measured.

Fluorescence resonance energy transfer

FRET between EGFP-UAP56 and mRFP SRm160 was measured using the Sensitized Emission FRET wizard in Leica SP2 confocal software. This software calculates FRET and FRET efficiency by the method of Gordon et al. (Gordon et al., 1998) after correction for any direct excitation of the acceptor at the donor excitation wavelength and after correcting for the dependence of FRET on the concentration of the acceptor.

In order to have the measured cell and the control cells in the same microscopic field and analyze the image, we separately transfected HeLa cells with EGFP-UAP56, with mRFP-SRm160, or with both. 24 hours later, transfected cells from all three cultures were trypsinized, mixed and replated on 22-mm coverslips for another 24 hours before fixation. The reference images from control cells expressing donor only (EGFP-UAP56) and acceptor only (mRFP-SRm160), and the FRET images from cells expressing both, were therefore collected simultaneously under identical optical conditions. Spectral overlap, optical cross-talk and differential expression levels of the fluorophores in the transfected cells were corrected for in the program by making measurements from the control cells in the same field (Gordon et al., 1998). The contributions of the background noise and spectral overlap were removed on a pixel-by-pixel basis in calculating the FRET signal in the doubly transfected cell in the same field. While collecting the images, the laser intensities were kept constant. Photomultiplier gain and offsets were selected so that fluorescence was within the linear range of detection, and this was checked for each control and FRET cell. EGFP was excited at 488 nm, whereas mRFP was excited with a laser line at 562 nm.

RNA interference

The siRNA duplexes (Smartpool, Dharmacon, Lafayette, CO) were transfected into HeLa cells using Oligofectamine (Invitrogen, Carlsbad, CA) as recommended by the manufacturer. siRNA duplexes, at a concentration of 10 nM, were introduced once on day 0 and again after 48 hours, and were assayed after 72 hours. For MCF-10A cells, an inducible knockdown was engineered using a two-lentivirus system (Szulc et al., 2006; Wiznerowicz and Trono, 2003) expressing an shRNA against UAP56 (Kapadia et al., 2006) under doxycycline induction. Cells were sorted for bicistronically expressed EGFP and dsRED and induced with 500 nm doxycycline. At 76 hours after doxycycline treatment, cell extracts were prepared and proteins were separated on 10% SDS PAGE gel. Western blotting was performed using affinity purified antibodies against UAP56.

Splicing reporter assay

RNA splicing was measured by a reporter assay in cells transfected with a human β-globin minigene, a generous gift from Benjamin Blencowe and Susan McCracken (McCracken et al., 2002). 293T cells were grown on 10-cm culture dishes to 90% confluence. 6 μg of β-globin-minigene-containing plasmid and 6 μg of EGFP-tagged UAP56 wt and/or UAP56 K95N were transfected into cells using 15 μl of Lipofectamine 2000 in serum-free Optimem. After 24 hours the cells were washed with PBS, and cytoplasmic and nuclear extracts were prepared with a Qiagen RNeasy kit according to kit instructions, except that the nuclear fraction was washed an extra time with 10 volumes of lysis buffer to minimize cytoplasmic contamination. After separating cytoplasmic and nuclear fractions, the total RNA from each fraction was extracted with 1 ml of TRIZOL (Invitrogen). Real-time PCR was performed using a DNA Engine Opticon System (MJ Research). The primers for β-globin minigene were in exon 1 and exon 2. The spliced or unspliced products were identified based on the molecular weight of real-time PCR product run on 1.2% agarose gel. The cDNA was amplified using a QIAGEN HotStarTaq Master Mix kit (QIAGEN) containing SYBR green (Schmittgen and Zakrajsek, 2000) and using 0.1 μg of the following primers: β-globin minigene forward primer, 5′-ATGGTGCATCTG-ACTCCT-3′; β-globin minigene reverse primer in exon 2, 5′-CCTGAAGTTCTC-AGGATC-3′.

The data presented are the mean values of three independently performed experiments.

ATP-binding assay

Binding of ATP to UAP56 or to the UAP56 K95N mutant was assayed by a method previously used for the DEAD-box helicase eIF4A (Pause and Sonenberg, 1992). Briefly, 1 μg of purified GST-UAP56 wt or GST-UAP56 K95N mutant were incubated with 2.5 μCi α-ATP P32 (3000 Ci/mmol) in 30 mM Tris-HCl (pH 7.5), 5 mM magnesium acetate, 10% glycerol and 1.5 mM DTT for 20 minutes at 37°C. ATP was cross-linked to the protein by irradiation with a 15 W Westinghouse Steri Germicidal UV lamp at 4°C, from a distance of 2 cm for 20 minutes. Cross-linking was done both in the presence and absence of 0.1 A260 units of PolyU (Sigma). After cross-linking, 4 mM unlabelled ATP was added to the reaction mixture. Finally, 20 μg of RNase A (Qiagen) was added to the reaction and incubated at 37°C for 10 minutes. The samples were then heated to 100°C in SDS PAGE loading buffer for 5 minutes, cooled down to room temperature and loaded on a 12.5% SDS-PAGE gel. After electrophoresis, the gel was dried, processed for autoradiography and quantified with a Storm phosphimager.

Statistical analysis

The equivalence of fluorescence curves was evaluated by what has been called the 'NIH' method (Feldman, 1988), i.e. fitting third-order polynomial regression curves to the time series data for each cell and then evaluating differences in means for the model coefficients between groups. The resulting model coefficients for each subject were compared overall between groups by multivariate analysis of variance (MANOVA) (Morrison, 1976). If there had been significant overall differences between groups by MANOVA, differences between groups for each coefficient (i.e. linear, quadratic and cubic) would have been evaluated using Student's *t*-tests.

We thank Susan McCracken and Ben Blencowe (University of Toronto) for reagents and help with splicing reporter assays; Ika Latz and Ted Giehl (UMass Medical School) for assistance with FRET studies; and Lee Johnson for providing GST constructs of UAP56 and URH49. We thank Stephen P. Baker (UMass Bioinformatics Unit) for help with statistical analysis. These studies were funded by the American Cancer Society and the National Cancer Institute.

References

Allcock, R. J., Williams, J. H. and Price, P. (2001). The central MHC gene, BAT1, may encode a protein that down-regulates cytokine production. *Genes Cells* **6**, 487-494.

Andersen, C. B., Ballut, L., Johansen, J. S., Chamieh, H., Nielsen, K. H., Oliveira, C. L., Pedersen, J. S., Seraphin, B., Le Hir, H. and Andersen, G. R. (2006). Structure of the exon junction core complex with a trapped DEAD-Box ATPase bound to RNA. *Science* **313**, 1968-1972.

Ballut, L., Marchadier, B., Baguet, A., Tomasetto, C., Seraphin, B. and Le Hir, H. (2005). The exon junction core complex is locked onto RNA by inhibition of eIF4AIII ATPase activity. *Nat. Struct. Mol. Biol.* **12**, 861-869.

Bernhard, W. (1969). A new staining procedure for electron microscopical cytology. *J. Ultrastruct. Res.* **27**, 250-265.

Biggiogera, M. and Fakan, S. (1998). Fine structural specific visualization of RNA on ultrathin sections. *J. Histochem. Cytochem.* **46**, 389-395.

Blencowe, B. J., Nickerson, J. A., Issner, R., Penman, S. and Sharp, P. A. (1994). Association of nuclear matrix antigens with exon-containing splicing complexes. *J. Cell Biol.* **127**, 593-607.

Blencowe, B. J., Issner, R., Nickerson, J. A. and Sharp, P. A. (1998). A coactivator of pre-mRNA splicing. *Genes Dev.* **12**, 996-1009.

Blencowe, B. J., Bauren, G., Eldridge, A. G., Issner, R., Nickerson, J. A., Rosonina, E. and Sharp, P. A. (2000). The SRm160/300 splicing coactivator subunits. *RNA* **6**, 111-120.

Calapez, A., Pereira, H. M., Calado, A., Braga, J., Rino, J., Carvalho, C., Tavanez, J. P., Wahle, E., Rosa, A. C. and Carmo-Fonseca, M. (2002). The intranuclear mobility of messenger RNA binding proteins is ATP dependent and temperature sensitive. *J. Cell Biol.* **159**, 795-805.

Chan, C. C., Dostie, J., Diem, M. D., Feng, W., Mann, M., Rappsilber, J. and Dreyfuss, G. (2004). eIF4A3 is a novel component of the exon junction complex. *RNA* **10**, 200-209.

Cheng, H., Dufu, K., Lee, C. S., Hsu, J. L., Dias, A. and Reed, R. (2006). Human mRNA export machinery recruited to the 5′ end of mRNA. *Cell* **127**, 1389-1400.

Cmarko, D., Verschure, P. J., Martin, T. E., Dahmus, M. E., Krause, S., Fu, X. D., van Driel, R. and Fakan, S. (1999). Ultrastructural analysis of transcription and splicing in the cell nucleus after bromo-UTP microinjection. *Mol. Biol. Cell* **10**, 211-223.

Culjkovic, B., Topisirovic, I., Skrabanek, L., Ruiz-Gutierrez, M. and Borden, K. L. (2006). eIF4E is a central node of an RNA regulon that governs cellular proliferation. *J. Cell Biol.* **175**, 415-426.

Custodio, N., Carvalho, C., Condado, I., Antoniou, M., Blencowe, B. J. and Carmo-Fonseca, M. (2004). In vivo recruitment of exon junction complex proteins to transcription sites in mammalian cell nuclei. *RNA* **10**, 622-633.

Feldman, H. A. (1988). Families of lines: random effects in linear regression analysis. *J. Appl. Physiol.* **64**, 1721-1732.

Ferreira, J. A., Carmo-Fonseca, M. and Lamond, A. I. (1994). Differential interaction of splicing snRNPs with coiled bodies and interchromatin granules during mitosis and assembly of daughter cell nuclei. *J. Cell Biol.* **126**, 11-23.

Fleckner, J., Zhang, M., Valcarcel, J. and Green, M. R. (1997). U2AF65 recruits a novel human DEAD box protein required for the U2 snRNP-branchpoint interaction. *Genes Dev.* **11**, 1864-1872.

Forler, D., Rabut, G., Ciccarelli, F. D., Herold, A., Kocher, T., Niggeweg, R., Bork, P., Ellenberg, J. and Izaurralde, E. (2004). RanBP2/Nup358 provides a major binding site for NXF1-p15 dimers at the nuclear pore complex and functions in nuclear mRNA export. *Mol. Cell. Biol.* **24**, 1155-1167.

Gatfield, D., Le Hir, H., Schmitt, C., Braun, I. C., Kocher, T., Wilm, M. and Izaurralde, E. (2001). The DExH/D box protein HEL/UAP56 is essential for mRNA nuclear export in Drosophila. *Curr. Biol.* **11**, 1716-1721.

Glauert, A. M. (1991). Fixatives. In *Fixation, Dehydration and Embedding of Biological Specimens*. Vol. 3, Pt 1 (ed. A. M. Glauert), p. 14. New York: Elsevier North-Holland Biomedical Press.

Gordon, G. W., Berry, G., Liang, X. H., Levine, B. and Herman, B. (1998). Quantitative fluorescence resonance energy transfer measurements using fluorescence microscopy. *Biophys. J.* **74**, 2702-2713.

Goshima, G., Wollman, R., Goodwin, S. S., Zhang, N., Scholey, J. M., Vale, R. D. and Stuurman, N. (2007). Genes required for mitotic spindle assembly in Drosophila S2 cells. *Science* **316**, 417-421.

Herold, A., Klymenko, T. and Izaurralde, E. (2001). NXF1/p15 heterodimers are essential for mRNA nuclear export in Drosophila. *RNA* **7**, 1768-1780.

Hodge, C. A., Colot, H. V., Stafford, P. and Cole, C. N. (1999). Rat8p/Dbp5p is a shuttling transport factor that interacts with Rat7p/Nup159p and Gle1p and suppresses the mRNA export defect of xpo1-1 cells. *EMBO J.* **18**, 5778-5788.

Jensen, T. H., Boulay, J., Rosbash, M. and Libri, D. (2001). The DECD box putative ATPase Sub2p is an early mRNA export factor. *Curr. Biol.* **11**, 1711-1715.

Jimeno, S., Rondon, A. G., Luna, R. and Aguilera, A. (2002). The yeast THO complex and mRNA export factors link RNA metabolism with transcription and genome instability. *EMBO J.* **21**, 3526-3535.

Kapadia, F., Pryor, A., Chang, T. H. and Johnson, L. F. (2006). Nuclear localization of poly(A)+ mRNA following siRNA reduction of expression of the mammalian RNA helicases UAP56 and URH49. *Gene* **384**, 37-44.

Kataoka, N., Yong, J., Kim, V. N., Velazquez, F., Perkinson, R. A., Wang, F. and Dreyfuss, G. (2000). Pre-mRNA splicing imprints mRNA in the nucleus with a novel RNA-binding protein that persists in the cytoplasm. *Mol. Cell* **6**, 673-682.

Kataoka, N., Diem, M. D., Kim, V. N., Yong, J. and Dreyfuss, G. (2001). Magoh, a human homolog of Drosophila mago nashi protein, is a component of the splicing-dependent exon-exon junction complex. *EMBO J.* **20**, 6424-6433.

Kiesler, E., Miralles, F. and Visa, N. (2002). HEL/UAP56 binds cotranscriptionally to the balbiani ring pre-mRNA in an intron-independent manner and accompanies the BR mRNP to the nuclear pore. *Curr. Biol.* **12**, 859-862.

Knight, D. P. (1982). Cytological staining methds in electron microscopy. In *Staining Methods for Sectioned Material*. Vol. 5, Pt 1 (ed. P. R. Lewis and D. P. Knight), pp. 44. New York: Elsevier North-Holland Biomedical Press.

Kruhlak, M. J., Lever, M. A., Fischle, W., Verdin, E., Bazett-Jones, D. P. and Hendzel, M. J. (2000). Reduced mobility of the Alternate Splicing Factor (ASF) through the nucleoplasm and steady state speckle compartments. *J. Cell Biol.* **150**, 41-52.

Lamond, A. I. and Spector, D. L. (2003). Nuclear speckles: a model for nuclear organelles. *Nat. Rev. Mol. Cell Biol.* **4**, 605-612.

Le Hir, H., Izaurralde, E., Maquat, L. E. and Moore, M. J. (2000a). The spliceosome deposits multiple proteins 20-24 nucleotides upstream of mRNA exon-exon junctions. *EMBO J.* **19**, 6860-6869.

Le Hir, H., Moore, M. J. and Maquat, L. E. (2000b). Pre-mRNA splicing alters mRNP composition: evidence for stable association of proteins at exon-exon junctions. *Genes Dev.* **14**, 1098-1108.

Lele, T. P. and Ingber, D. E. (2006). A mathematical model to determine molecular kinetic rate constants under non-steady state conditions using fluorescence recovery after photobleaching (FRAP). *Biophys. Chem.* **120**, 32-35.

Lele, T., Oh, P., Nickerson, J. A. and Ingber, D. E. (2004). An improved mathematical approach for determination of molecular kinetics in living cells with FRAP. *Mech. Chem. Biosyst.* **1**, 181-190.

Lele, T., Wagner, S. R., Nickerson, J. A. and Ingber, D. E. (2006). Methods for measuring rates of protein binding to insoluble scaffolds in living cells: histone H1-chromatin interactions. *J. Cell. Biochem.* **99**, 1334-1342.

Libri, D., Graziani, N., Saguez, C. and Boulay, J. (2001). Multiple roles for the yeast SUB2/yUAP56 gene in splicing. *Genes Dev.* **15**, 36-41.

Liu, F., Wagner, S., Campbell, R. B., Nickerson, J. A., Schiffer, C. A. and Ross, A. H. (2005). PTEN enters the nucleus by diffusion. *J. Cell. Biochem.* **96**, 221-234.

Longman, D., Johnstone, I. L. and Caceres, J. F. (2003). The Ref/Aly proteins are dispensable for mRNA export and development in Caenorhabditis elegans. *RNA* **9**, 881-891.

Luo, M. J. and Reed, R. (1999). Splicing is required for rapid and efficient mRNA export in metazoans. *Proc. Natl. Acad. Sci. USA* **96**, 14937-14942.

Luo, M. L., Zhou, Z., Magni, K., Christoforides, C., Rappsilber, J., Mann, M. and Reed, R. (2001). Pre-mRNA splicing and mRNA export linked by direct interactions between UAP56 and Aly. *Nature* **413**, 644-647.

MacMorris, M., Brocker, C. and Blumenthal, T. (2003). UAP56 levels affect viability and mRNA export in Caenorhabditis elegans. *RNA* **9**, 847-857.

Masuda, S., Das, R., Cheng, H., Hurt, E., Dorman, N. and Reed, R. (2005). Recruitment of the human TREX complex to mRNA during splicing. *Genes Dev.* **19**, 1512-1517.

McCracken, S., Lambermon, M. and Blencowe, B. J. (2002). SRm160 splicing coactivator promotes transcript 3′-end cleavage. *Mol. Cell. Biol.* **22**, 148-160.

McCracken, S., Longman, D., Marcon, E., Moens, P., Downey, M., Nickerson, J. A., Jessberger, R., Wilde, A., Caceres, J. F., Emili, A. et al. (2005). Proteomic analysis

of SRm160-containing complexes reveals a conserved association with cohesin. *J. Biol. Chem.* **280**, 42227-42236.
Meshorer, E., Yellajoshula, D., George, E., Scambler, P. J., Brown, D. T. and Misteli, T. (2006). Hyperdynamic plasticity of chromatin proteins in pluripotent embryonic stem cells. *Dev. Cell* **10**, 105-116.
Mintz, P. J., Patterson, S. D., Neuwald, A. F., Spahr, C. S. and Spector, D. L. (1999). Purification and biochemical characterization of interchromatin granule clusters. *EMBO J.* **18**, 4308-4320.
Monneron, A. and Bernhard, W. (1969). Fine structural organization of the interphase nucleus in some mammalian cells. *J. Ultrastruct. Res.* **27**, 266-288.
Morrison, D. F. (1976). *Multivariate Statistical Methods*. New York: McGraw-Hill Book Company.
Nair, S., Dey, R., Sanford, J. P. and Doyle, D. (1992). Molecular cloning and analysis of an eIF-4A-related rat liver nuclear protein. *J. Biol. Chem.* **267**, 12928-12935.
Nickerson, J. A. (1998). Nuclear dreams: the malignant alteration of nuclear architecture. *J. Cell. Biochem.* **70**, 172-180.
Nickerson, J. A., Krockmalnic, G., He, D. C. and Penman, S. (1990). Immunolocalization in three dimensions: immunogold staining of cytoskeletal and nuclear matrix proteins in resinless electron microscopy sections. *Proc. Natl. Acad. Sci. USA* **87**, 2259-2263.
Pause, A. and Sonenberg, N. (1992). Mutational analysis of a DEAD box RNA helicase: the mammalian translation initiation factor eIF-4A. *EMBO J.* **11**, 2643-2654.
Peelman, L. J., Chardon, P., Nunes, M., Renard, C., Geffrotin, C., Vaiman, M., Van Zeveren, A., Coppieters, W., van de Weghe, A., Bouquet, Y. et al. (1995). The BAT1 gene in the MHC encodes an evolutionarily conserved putative nuclear RNA helicase of the DEAD family. *Genomics* **26**, 210-218.
Phair, R. D. and Misteli, T. (2000). High mobility of proteins in the mammalian cell nucleus. *Nature* **404**, 604-609.
Phair, R. D., Scaffidi, P., Elbi, C., Vecerova, J., Dey, A., Ozato, K., Brown, D. T., Hager, G., Bustin, M. and Misteli, T. (2004). Global nature of dynamic protein-chromatin interactions in vivo: three-dimensional genome scanning and dynamic interaction networks of chromatin proteins. *Mol. Cell. Biol.* **24**, 6393-6402.
Pryor, A., Tung, L., Yang, Z., Kapadia, F., Chang, T. H. and Johnson, L. F. (2004). Growth-regulated expression and G0-specific turnover of the mRNA that encodes URH49, a mammalian DExH/D box protein that is highly related to the mRNA export protein UAP56. *Nucleic Acids Res.* **32**, 1857-1865.
Reed, R. and Cheng, H. (2005). TREX, SR proteins and export of mRNA. *Curr. Opin. Cell Biol.* **17**, 269-273.
Saitoh, N., Spahr, C. S., Patterson, S. D., Bubulya, P., Neuwald, A. F. and Spector, D. L. (2004). Proteomic analysis of interchromatin granule clusters. *Mol. Biol. Cell* **15**, 3876-3890.
Schmidt, U., Richter, K., Berger, A. B. and Lichter, P. (2006). In vivo BiFC analysis of Y14 and NXF1 mRNA export complexes: preferential localization within and around SC35 domains. *J. Cell Biol.* **172**, 373-381.
Schmittgen, T. D. and Zakrajsek, B. A. (2000). Effect of experimental treatment on housekeeping gene expression: validation by real-time, quantitative RT-PCR. *J. Biochem. Biophys. Methods* **46**, 69-81.
Shamsher, M. K., Ploski, J. and Radu, A. (2002). Karyopherin beta 2B participates in mRNA export from the nucleus. *Proc. Natl. Acad. Sci. USA* **99**, 14195-14199.
Shi, H., Cordin, O., Minder, C. M., Linder, P. and Xu, R. M. (2004). Crystal structure of the human ATP-dependent splicing and export factor UAP56. *Proc. Natl. Acad. Sci. USA* **101**, 17628-17633.
Shopland, L. S., Johnson, C. V. and Lawrence, J. B. (2002). Evidence that all SC-35 domains contain mRNAs and that transcripts can be structurally constrained within these domains. *J. Struct. Biol.* **140**, 131-139.
Smith, K. P., Moen, P. T., Wydner, K. L., Coleman, J. R. and Lawrence, J. B. (1999). Processing of endogenous pre-mRNAs in association with SC-35 domains is gene specific. *J. Cell Biol.* **144**, 617-629.
Snay-Hodge, C. A., Colot, H. V., Goldstein, A. L. and Cole, C. N. (1998). Dbp5p/Rat8p is a yeast nuclear pore-associated DEAD-box protein essential for RNA export. *EMBO J.* **17**, 2663-2676.
Spies, T., Blanck, G., Bresnahan, M., Sands, J. and Strominger, J. L. (1989a). A new cluster of genes within the human major histocompatibility complex. *Science* **243**, 214-217.
Spies, T., Bresnahan, M. and Strominger, J. L. (1989b). Human major histocompatibility complex contains a minimum of 19 genes between the complement cluster and HLA-B. *Proc. Natl. Acad. Sci. USA* **86**, 8955-8958.
Staley, J. P. and Guthrie, C. (1998). Mechanical devices of the spliceosome: motors, clocks, springs, and things. *Cell* **92**, 315-326.
Stenoien, D. L., Patel, K., Mancini, M. G., Dutertre, M., Smith, C. L., O'Malley, B. W. and Mancini, M. A. (2001). FRAP reveals that mobility of oestrogen receptor-alpha is ligand- and proteasome-dependent. *Nat. Cell Biol.* **3**, 15-23.
Strahm, Y., Fahrenkrog, B., Zenklusen, D., Rychner, E., Kantor, J., Rosbach, M. and Stutz, F. (1999). The RNA export factor Gle1p is located on the cytoplasmic fibrils of the NPC and physically interacts with the FG-nucleoporin Rip1p, the DEAD-box protein Rat8p/Dbp5p and a new protein Ymr 255p. *EMBO J.* **18**, 5761-5777.
Strasser, K. and Hurt, E. (2001). Splicing factor Sub2p is required for nuclear mRNA export through its interaction with Yra1p. *Nature* **413**, 648-562.
Szulc, J., Wiznerowicz, M., Sauvain, M. O., Trono, D. and Aebischer, P. (2006). A versatile tool for conditional gene expression and knockdown. Nat. *Methods* **3**, 109-116.
Tange, T. O., Shibuya, T., Jurica, M. S. and Moore, M. J. (2005). Biochemical analysis of the EJC reveals two new factors and a stable tetrameric protein core. *RNA* **11**, 1869-1883.
Tanner, N. K. and Linder, P. (2001). DExD/H box RNA helicases: from generic motors to specific dissociation functions. *Mol. Cell* **8**, 251-262.
Tseng, S. S., Weaver, P. L., Liu, Y., Hitomi, M., Tartakoff, A. M. and Chang, T. H. (1998). Dbp5p, a cytosolic RNA helicase, is required for poly(A)+ RNA export. *EMBO J.* **17**, 2651-2662.
Wagner, S., Chiosea, S. and Nickerson, J. A. (2003). The spatial targeting and nuclear matrix binding domains of SRm160. *Proc. Natl. Acad. Sci. USA* **100**, 3269-3274.
Wagner, S., Chiosea, S., Ivshina, M. and Nickerson, J. A. (2004). In vitro FRAP reveals the ATP-dependent nuclear mobilization of the exon junction complex protein SRm160. *J. Cell Biol.* **164**, 843-850.
Wan, K. M., Nickerson, J. A., Krockmalnic, G. and Penman, S. (1994). The B1C8 protein is in the dense assemblies of the nuclear matrix and relocates to the spindle and pericentriolar filaments at mitosis. *Proc. Natl. Acad. Sci. USA* **91**, 594-598.
Wiznerowicz, M. and Trono, D. (2003). Conditional suppression of cellular genes: lentivirus vector-mediated drug-inducible RNA interference. *J. Virol.* **77**, 8957-8961.
Zhang, M. and Green, M. R. (2001). Identification and characterization of yUAP/Sub2p, a yeast homolog of the essential human pre-mRNA splicing factor hUAP56. *Genes Dev.* **15**, 30-35.
Zhao, J., Jin, S. B., Bjorkroth, B., Wieslander, L. and Daneholt, B. (2002). The mRNA export factor Dbp5 is associated with Balbiani ring mRNP from gene to cytoplasm. *EMBO J.* **21**, 1177-1187.
Zhao, R., Shen, J., Green, M. R., MacMorris, M. and Blumenthal, T. (2004). Crystal structure of UAP56, a DExD/H-box protein involved in pre-mRNA splicing and mRNA export. *Structure* **12**, 1373-1381.